Supplemental Information

S1 Electrostatic energy

We here further discuss the expressions for U_{ET} reported in Sec.2 for either a MFMIM or a MFIM capacitor. For both systems the starting point is the U_{ET} definition in Eq.3.

As already mentioned in the main text, in the MFMIM capacitor the ferroelectric and dielectric fields are independent of $\bar{r}=(x,y)$ and we have $E_{F,T}=(C_D V_T - P_{AV})/(t_F C_0)$, $V_D=(C_F V_T + P_{AV})/C_0$,[1] where $P_{AV}=(\sum_{j=1}^{n_D} P_j)/n_D$ is the average polarisation. By substituting the $E_{F,T}$ and V_D expressions in Eq.3 we obtain

$$\begin{aligned} U_{ET} &= -\frac{V_T}{2}\frac{A}{d^2}\frac{C_F}{C_0}(C_D V_T - P_{AV}) - V_T \sum_{j=1}^{n_D} P_j + \frac{n_D P_{AV}}{2C_0}(C_F V_T + P_{AV}) \\ &= \frac{n_D P_{AV}^2}{2C_0} - \frac{C_s V_T^2}{2} n_D - n_D \frac{C_D}{C_0} V_T P_{AV} \end{aligned} \tag{S1}$$

where the total device area is $A=n_D d^2$ and we grouped terms proportional to P_{AV}^2, V_T^2 and $V_T P_{AV}$. Eq.S1 coincides with Eq.6, with the depolarisation energy U_{dep} for the MFMIM system defined in Eq.7.

In the MFIM structure the calculation of the ferroelectic and dielectric field is a three-dimensional problem, that we can approach by recalling that V_T and each spontaneous polarisation P_h are the sources of the electric fields. Because the system is linear, the superposition of effects allows us to write

$$E_{F,T}(\bar{r}) = \sum_{h=1}^{n_D} P_h G_{FT,h}(\bar{r}) + \frac{C_D V_T}{t_F C_0} \tag{S2}$$

where $G_{FT,h}(\bar{r})$ is the Green's function for the field $E_{F,T}(\bar{r})=E_{F,z}(\bar{r},-t_F)$ of a unitary charge per unit area in domain h, while the effect of V_T is simply described by a capacitor divider. We can similarly write the potential $V_D(\bar{r})$ as

$$V_D(\bar{r}) = \sum_{h=1}^{n_D} P_h G_{D,h}(\bar{r}) + \frac{C_F}{C_0} V_T \tag{S3}$$

where $G_{D,h}(\bar{r})$ is the Green's function for $V_D(\bar{r})$ of a unitary charge in domain h. By substituting Eqs.S2, S3 in Eq.3 we recognise that the calculation of U_{ET} entails the evaluation of the integral of any $G_{D,h}$ over any domain area D_j, and of any $G_{FT,h}(\bar{r})$ over the device area A. Consequently we introduce the capacitances

$$\frac{1}{C_{j,h}} = \frac{1}{d^2}\int_{D_j} G_{D,h}(\bar{r}) d\bar{r} \tag{S4}$$

as well as the adimensional coefficients

$$B_h = \frac{\varepsilon_0 \varepsilon_F}{d^2}\int_A G_{FT,h}(\bar{r}) d\bar{r} \tag{S5}$$

which allow us to write the U_{ET} of the MFIM system as

$$U_{ET} = \frac{1}{2}\sum_{j,h=1}^{n_D} \frac{P_h P_j}{C_{j,h}} - \frac{V_T}{2}\sum_{h}^{n_D} P_h (B_h + 1 + C_D/C_0) - \frac{C_S V_T^2}{2} n_D \ . \tag{S6}$$

By the definition of $C_{j,h}$ we see that by summing over h we obtain the Green's function for $V_D(\bar{r})$ in domain j of a uniform charge in the entire device area, so that we have

$$\sum_{h=1}^{n_D} \frac{1}{C_{j,h}} = \frac{1}{C_0}, \qquad \sum_{j,h=1}^{n_D} \frac{1}{C_{j,h}} = \frac{n_D}{C_0} \tag{S7}$$

where the second equality is due to the fact that the first sum is independent of the domain j.

In consideration of the Neumann boundary conditions used for the electric field at the edges of the MFIM structure (see Supplementary Section S7), analytical derivations suggest and numerical calculations confirm that the B_h defined in Eq.S5 evaluates to $B_h \simeq -C_F/C_0$ and it is independent of h (not shown). By substituting $B_h \simeq -C_F/C_0$ in Eq.S6, we obtain the U_{ET} expression for the MFIM capacitor given by Eq.6, with the depolarisation energy U_{dep} defined in Eq.7.

For all the MIFM systems analysed in this work the capacitances $C_{j,h}$ were evaluated numerically and then used in all analyses. More details about the three-dimensional calculations of the capacitances are given in Supplementary Section S7.

S2 Conditions for a stable NC operation in a MFMIM system

For convenience of notation we here introduce $\theta = (t_F k)/(dw)$ and $\eta = 1/C_0$. Given the Laplacian matrix $\mathbf{L}$ and the all-one matrix $\mathbf{O}_{dep}$, both having size n_D, we prove that

$$\sigma_{min}\left[\theta\mathbf{L} + \eta\frac{\mathbf{O}_{dep}}{n_D}\right] = \min\{\eta, \theta\sigma_1(\mathbf{L})\} \tag{S8}$$

where $\sigma_{min}[M]$ denotes the smallest eigenvalue of matrix M and $\sigma_1(\mathbf{L})$ denotes the second smallest eigenvalue of the Laplacian $\mathbf{L}$.

The eigenvalues of matrix $\frac{\mathbf{O}_{dep}}{n_D}$ are 1, and 0 with multiplicity $n_D - 1$. Since the graph is connected, $\mathbf{L}$ has an eigenvalue 0 with multiplicity 1, while all the other eigenvalues $\sigma_1(\mathbf{L}) \leq \sigma_2(\mathbf{L}) \leq \cdots \leq \sigma_{n_D-1}(\mathbf{L})$ are real and positive. Matrix $\mathbf{L}$ and matrix $\frac{\mathbf{O}_{dep}}{n_D}$ share the normalised eigenvector $v = \frac{\mathbf{1}_{n_D}}{\sqrt{n_D}}$ (where $\mathbf{1}_{n_D}$ denotes an all-one vector of size n_D), which is associated with the 0 eigenvalue of $\mathbf{L}$ (i.e. $\mathbf{L}v = 0$) and with the 1 eigenvalue of $\frac{\mathbf{O}_{dep}}{n_D}$ (i.e. $\frac{\mathbf{O}_{dep}}{n_D}v = v$).

Let us complement vector v with matrix $V \in \mathbb{R}^{n_D \times n_D - 1}$ to obtain an orthonormal matrix $T = \begin{bmatrix} v & V \end{bmatrix}$ (such that $T^{-1} = T^\top$). We can then apply this transformation to simultaneously diagonalise both matrices:

$$T^{-1}(\theta\mathbf{L} + \eta\frac{\mathbf{O}_{dep}}{n_D})T = \begin{bmatrix} v^\top \\ V^\top \end{bmatrix}(\theta\mathbf{L} + \eta\frac{\mathbf{O}_{dep}}{n_D})\begin{bmatrix} v & V \end{bmatrix} \tag{S9}$$

$$= \begin{bmatrix} 0 & \mathbf{0}_{n_D-1}^\top \\ \mathbf{0}_{n_D-1} & \theta\Lambda \end{bmatrix} + \begin{bmatrix} \eta & \mathbf{0}_{n_D-1}^\top \\ \mathbf{0}_{n_D-1} & \bar{\mathbf{0}}_{n_D-1} \end{bmatrix}, \tag{S10}$$

where $\mathbf{0}_{n_D-1}$ denotes an all-zero vector of size $n_D - 1$, $\bar{\mathbf{0}}_{n_D-1}$ an all-zero matrix of size $n_D - 1$, and $\Lambda = \text{diag}\{\sigma_1(\mathbf{L}), \ldots, \sigma_{n_D-1}(\mathbf{L})\}$ is the diagonal matrix carrying on the diagonal the nonzero eigenvalues of $\mathbf{L}$. It is then clear that the spectrum of $\theta\mathbf{L} + \eta\frac{\mathbf{O}_{dep}}{n_D}$ is the union of η and of the nonzero scaled Laplacian eigenvalues $\theta\sigma_1(\mathbf{L}), \ldots, \theta\sigma_{n_D-1}(\mathbf{L})$. Therefore, the smallest eigenvalue is the minimum between η and $\theta\sigma_1(\mathbf{L})$. By recalling that, for the Laplacian matrix corresponding to a rectangular grid, $\sigma_1(\mathbf{L}) = [2\sin(\pi/(2\sqrt{n_D}))]^2$, we obtain

$$\sigma_{min}\left[\frac{t_F k}{dw}\mathbf{L} + \frac{\mathbf{O}_{dep}}{n_D C_0}\right] = \min\left\{\frac{1}{C_0}\,,\ \frac{t_F k}{dw}[2\sin(\pi/(2\sqrt{n_D}))]^2\right\} \tag{S11}$$

that proves the stability condition in Eq.12.

S3 Conditions for a stable NC operation in a MFIM system

In the MFIM case the condition for a stable NC operation is given by Eq.11c, where $\mathbf{C}_{dep}$ is defined in Eq.10. We argue that $\mathbf{C}_{dep}$ has a large influence on the spectrum of the Jacobian matrix for the MFIM system, in fact $\mathbf{C}_{dep}$ can modify all the eigenvalues of $\mathbf{C}_{dep} + \mu\mathbf{L}$, where $\mu = \frac{t_F k}{dw}$. We have a necessary condition for stability in terms of the entries of $\mathbf{C}_{dep}$. In fact, we notice that Eq.11c requires that the inequality $P^\top[\mathbf{C}_{dep} + \mu\mathbf{L}]P > 2|\alpha|t_F\|P\|^2 > 0$ be fulfilled for all nonzero P vectors. We now take $P = \bar{1}^\top = [1\ 1\ 1\ \ldots 1]^\top$, such that $\|P\|^2 = n_D$. Exploiting the fact that $\bar{1}^\top\mathbf{L}\bar{1} = 0$, we obtain

$$\frac{\bar{1}^\top[\mathbf{C}_{dep} + \mu\mathbf{L}]\bar{1}}{n_D} = \frac{\bar{1}^\top\mathbf{C}_{dep}\bar{1}}{n_D} = \frac{\sum_{i,j=1}^{n_D}\mathbf{C}_{dep}(i,j)}{n_D} > 2|\alpha|t_F. \tag{S12}$$

In view of the sum rule in Eq.S7, $\sum_{i,j=1}^{n_D} \mathbf{C}_{dep}(i,j) = n_D/C_0$, the above inequality becomes

$$\frac{1}{C_0} > 2|\alpha| t_F \ . \tag{S13}$$

Eq.S13 provides a necessary condition for a stable NC operation of the MFIM system.

S4 Stability of the equilibrium for $V_T \neq 0$

Here we discuss how the stability conditions discussed in Sec.3 for the condition all P_i=0 and V_T=0, in fact ensure stability for any V_T and corresponding P_i configurations. All the dynamic systems in Eqs.8a, 8b and 8c can be recast into the common form

$$\frac{dP}{dt} = \mathbf{A}P + \mathbf{f}(P) + \mathbf{1}u, \tag{S14}$$

where $\mathbf{A}$ is a symmetric matrix, the vector function $\mathbf{f}(P)$ has polynomial components

$$\mathbf{f}_i(P_i) = -\left(2\alpha P_i + 4\beta P_i^3 + 6\gamma P_i^5\right)/\rho,$$

$\mathbf{1}$ is a vector of all ones, and the constant u can be either $u = \frac{1}{t_F\rho} V_T$ (in the MFM case) or $u = \frac{1}{t_F\rho}(C_D/C_0)V_T$ (in the MFMIM and MFIM cases). The Jacobian of the system in Eq.S14, computed at the generic equilibrium point $\bar{P}$, is

$$\mathbf{J}(P) = \mathbf{A} - 2\alpha/\rho\mathbf{I} - \mathbf{diag}\{12\beta\bar{P}_i^2 + 30\bar{P}_i^4\}/\rho = \mathbf{J}(0) - \mathbf{D},$$

where the symmetric matrix $\mathbf{J}(0) = \mathbf{A} - 2\alpha/\rho\mathbf{I}$ is the Jacobian computed at the equilibrium $\bar{P}_i = 0$ (shown in Eqs.9a, 9b and 9c for the three different cases), while the diagonal matrix $\mathbf{D} = \mathbf{diag}\{12\beta\bar{P}_i^2 + 30\bar{P}_i^4\}$ has nonnegative diagonal entries because $\beta > 0$ and $\gamma \geq 0$.

Now, assume that the symmetric Jacobian $\mathbf{J}(0)$ has negative eigenvalues or, equivalently, that it is negative definite: $x^\top \mathbf{J}(0)x < 0$ for any vector $x \neq 0$. Then, also matrix $\mathbf{J}(P)$ is negative definite, because $x^\top \mathbf{J}x = x^\top \mathbf{J}(0)x - x^\top \mathbf{D}x \leq x^\top \mathbf{J}(0)x < 0$ for $x \neq 0$. Therefore, $\mathbf{J}(P)$ has negative eigenvalues.

Hence, to ensure the stability of all possible equilibria with a generic V_T, it is enough to guarantee the stability of the equilibrium $P_i = 0$ corresponding to $V_T = 0$, which is discussed in the main paper.

S5 Statistical dispersion of the ferroelectric anisotropy constants

In actual ferroelectric materials the anisotropy constants α, β and γ may have domain to domain variations, and it has been argued also that, by accounting for such a statistical dispersion, simulations can improve the agreement with experiments in the analysis of metal-ferroelectric-metal systems.[9]

A straightforward extension of the stability analysis in Sec.3 shows that, in the presence of a statistical dispersion of α, stability conditions can still be expressed as in Eqs.11 if we substitute $|\alpha|$ in right hand side of the equations with α_{max}, here defined as the maximum $|\alpha_i|$, with $i = 1,2\ldots,n_D$ being an index identifying domains. If we consider a system consisting of many domains with an average value, $|\alpha|_{av}$, of the $|\alpha_i|$ constants, the introduction of α_{max} in the inequalities of Eqs.11 inherently implies a more stringent requirement for a stable NC operation compared to the same system with a negligible dispersion.

We introduced in our analysis a randomness of α_i, β_i constants (still keeping γ=0) and revisited some of the results in Fig.2 for a MFIM system. In order to have a clear physical interpretation of the statistical dispersion in the system, our starting point is a statistical dispersion of the ferroelectric coercive field E_C. More precisely, we used a random generation of the coercive field $E_{C,i}$ in each domain by using a gaussian distribution of E_C with a mean value $E_{C,av}$=0.54 MV/cm (corresponding to α=$-4.6\cdot10^8$ m/F and β=$9.8\cdot10^9$ m^5/C^2/F, see the beginning of Sec.3), and for different standard deviations $E_{C,dev}$. Then for each $E_{C,i}$ we calculated the corresponding α_i, β_i by using the analytical expressions α_i=$-3\sqrt{3}E_c/(2P_r)$, β_i=$3\sqrt{3}E_c/(2P_r^3)$, which hold for γ=0;[2] no dispersion of the remnant polarisation P_r was considered in the calculations. The eigenvalues of the Jacobian matrices were calculated numerically in the condition of all P_i=0.

Fig.S1(a) shows an analysis similar to Fig.2(b) but for a fixed Ta_2O_5 thickness t_D=13.5 nm and accounting for a statistical dispersion of α_i, β_i. In the presence of such a statistical dispersion, each MFIM capacitor is a

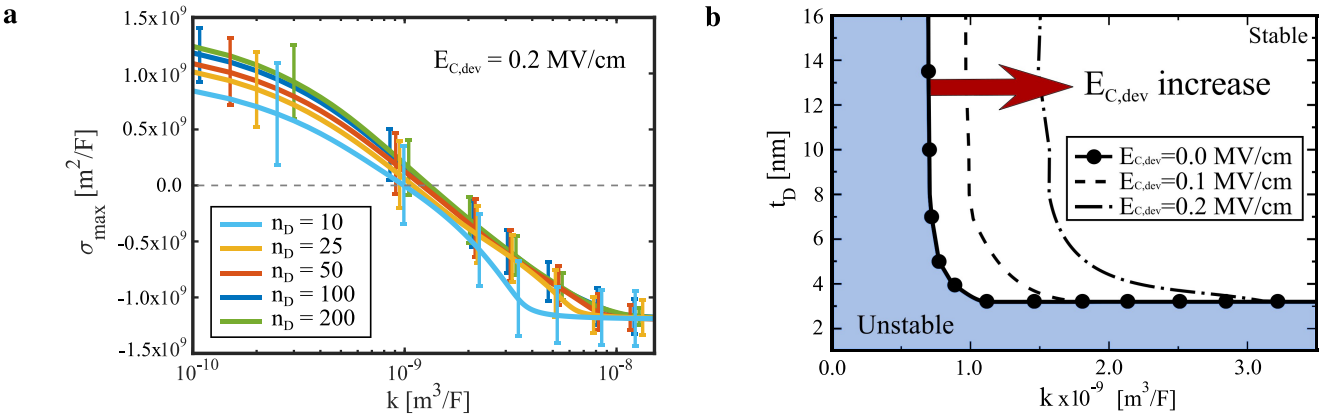

Figure S1: **Eigenvalues of the Jacobian matrix and design space for stable NC operation in the presence of statistical dispersion of the anisotropy constants**: **a.** Maximum eigenvalue σ_{max} of the Jacobian matrix for a $Hf_{0.5}Zr_{0.5}O_2-Ta_2O_5$ MFIM structure (in the condition of all P_i=0) versus the domain wall coupling factor k. Calculations account for a statistical dispersion of α, β stemming from a standard deviation $E_{C,dev}$=0.2 MV/cm of the coercive field and correspond to 100 realizations of the MFIM structure. Lines show the σ_{max} averaged between the realizations, while the error bar symbols indicate the range between minimum and maximum σ_{max} among the different realizations at some k values. Results are shown for different values of the domain number n_D, and all parameters other than n_D, α, β are the same as in calculations for t_D=13.5 nm in Fig.2(c). **b.** Regions for stable NC operation for a MFIM structure in the t_D versus k plane and for different standard deviation $E_{C,dev}$ of the coercive field. All parameters other than n_D, α, β are the same as in Fig.2 for the case t_D=13.5 nm, t_F=11.6 nm. Area A=2500nm^2 and n_D=100.

statistical realization of a stochastic process and has a distinct set of eigenvalues of the Jacobian matrix, whose values depend also on the number n_D of domains. Fig.S1(a) illustrates σ_{max} for a standard deviation $E_{C,dev}$=0.2 MV/cm of the coercive field, for 100 realizations and for different n_D values. For each domain wall coupling factor k the figure reports the σ_{max} averaged between the realizations (lines), and for some k values the figure also shows the range between minimum and maximum σ_{max} among the different realizations. As it can be seen the average σ_{max} converges quite quickly by increasing n_D. Fig.S1(a) also shows that larger k values are required for a stable NC operation for increasing $E_{C,dev}$. This latter aspect is better illustrated in Fig.S1(b), that revisits the analysis in Fig.2(d) for t_F=11.6nm and for different standard deviation $E_{C,dev}$ of the coercive field.

The results in Fig.S1(b) show a qualitative trend indicating that a statistical dispersion of the anisotropy constants results in more stringent requirements for the k values necessary for a stable NC operation. In the presence of such a statistical dispersion, one should more appropriately discuss the probability of a stable NC operation in a given MFIM system, however such a statistical analysis of the stability properties goes beyond the scope of the present work.

S6 Influence of interface traps on the stability conditions of a MFIM system

The possible presence of traps at the ferroelectric-dielectric interface has an influence on NC stabilization because traps can partly screen the ferroelectric polarisation, which has an inherently destabilizing effect. Let us consider a number, N_E, of discrete trap levels in each domain, denote with $E_{Tr,i}$ a trap energy in the domain i (with Tr=1,2,...,N_E and i=1,2,...,n_D), and indicate with Q_T the charge density per unit area due to traps. The present analysis is developed for a MFIM system, so that we can use a straightforward modification of Eq.8c and write the overall dynamic system as

$$t_F \rho \frac{dP_i}{dt} = \partial U_{LGD} - \frac{1}{2}\sum_{j=1}^{n_D}\left[\frac{1}{C_{i,j}}+\frac{1}{C_{j,i}}\right](P_j+Q_{T,j}) + \frac{C_D}{C_0}V_T(t) \tag{S15a}$$

$$\frac{\partial n_{Tr,i}}{\partial t} = c_n\,(N_t - n_{Tr,i}) - e_n\,n_{Tr,i} \tag{S15b}$$

where $n_{Tr,i}$ is the density of electrons trapped at energy E_{Tr} in domain i, while N_t is the corresponding trap density. Here the emission rate is e_n=$e_{n0}\,F_0[(E_{f,B}-E_{Tr})/K_BT]$, where e_{n0} is a bias independent rate and $F_0(\eta)$ is the Fermi-Dirac equilibrium occupation function[3]. Hence e_n depends on the external bias V_T via the position of E_{Tr} with

[3]The Fermi-Dirac occupation function $F_0(\eta)$ is defined as $F_0(\eta)$=$1/[1+\exp(\eta)]$.

respect to $E_{f,B}$ and, in particular, it is equal to e_{n0} when E_{Tr} is at least a few K_BT above $E_{f,B}$, whereas it decays exponentially for decreasing E_{Tr} when E_{Tr} is below $E_{f,B}$. The capture rate c_n is expressed as $c_n{=}e_n \exp[(E_{fB} - E_{Tr})/K_BT]$ so that, according to Eq.S15b, the steady-state occupation of traps is in thermodynamic equilibrium with $E_{f,B}$. The system in Eqs.S15 consists of $n_D{+}n_D \cdot N_E$ equations, hence the inclusion of traps substantially increases the size of the problem.

The e_n, c_n expressions couple Eq.S15b to Eq.S15a because $E_{Tr,i}$ depends on the average voltage $V_{D,i}$ at the ferroelectric-dielectric interface in the domain i. An explicit expression of the coupling between Eq.S15a and Eq.S15b is given by

$$Q_{T,i} = \Delta E \sum_{Tr=1}^{N_E} (-q)\, n_{Tr,i} \tag{S16a}$$

$$E_{Tr,i} = \Phi_M - (\chi_D + E_0 - i\Delta E) - qV_{D,i} \tag{S16b}$$

$$V_{D,i} = \sum_{j=1}^{n_D} \frac{(P_j + Q_{T,j})}{C_{i,j}} + \frac{C_F}{C_0} V_T(t) \tag{S16c}$$

where $E_{Tr,i}$ is the trap energy referred to E_{fB} (see Fig.4(e)). Here Φ_M and χ_D are respectively the metal gate work-function and dielectric electron affinity, E_0 is the depth into the dielectric bandgap of the deepest trap, ΔE is the energy step between the discrete trap levels, and Eq.S16a assumes traps are acceptor type.

Eqs.S15 and S16 summarize the model that we used for the simulations in Fig.4(f), and in this section we more formally study the stable NC operation by inspecting the sign of the Jacobian matrix of Eqs.S15. In this respect, Fig.S2(a) shows an analysis similar to Fig.2(c) but for a fixed Ta_2O_5 thickness t_D=5nm and different uniform trap densities N_T at the $Hf_{0.5}Zr_{0.5}O_2{-}Ta_2O_5$ interface. As it can be seen, by increasing N_T the σ_{max} at large k values progressively increase and the system is eventually driven to instability for a large enough N_T. It is worth noting that the impact on σ_{max} of an increase of N_T in Fig.S2(a) is qualitatively similar to the impact of a t_D reduction in Fig.2(c). This can be intuitively explained by arguing that the trap capacitance $C_{it}{=}q^2N_T$ goes in parallel to C_D, thus increasing the effective dielectric capacitance and eventually precluding the NC stabilization. This is confirmed by Fig.S2(b), showing that the charge versus ferroelectric field curves of the MFIM capacitor tend to deviate from the NC region when N_T increases, with a behavior qualitatively similar to the results in Fig.4(f) where the pulse width of the trapezoidal input waveform was varied at fixed N_T.

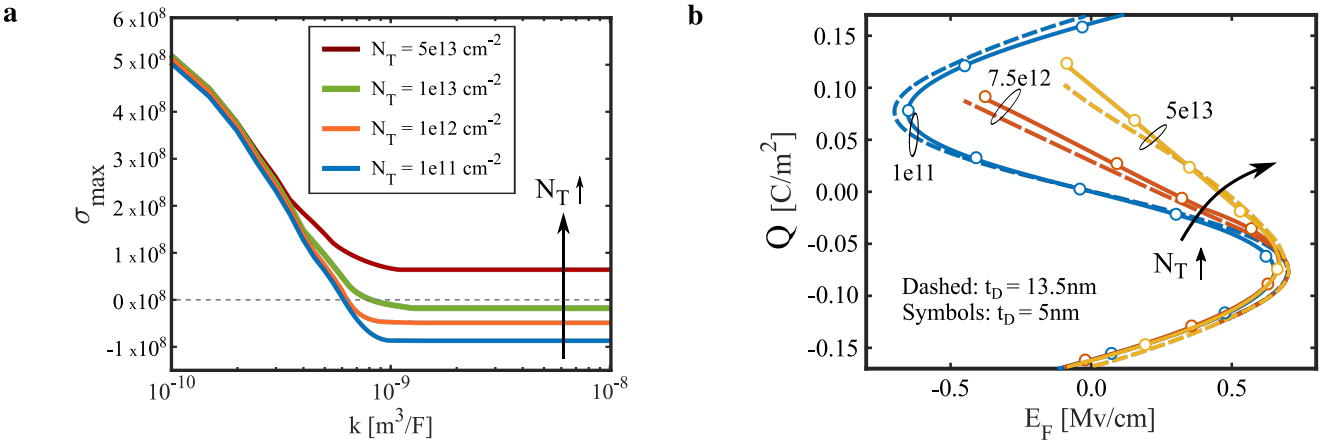

Figure S2: **Eigenvalues of the Jacobian matrix and stable NC operation in the presence of interface traps**: **a.** Maximum eigenvalue σ_{max} of the Jacobian matrix (for all P_i=0) of a $Hf_{0.5}Zr_{0.5}O_2{-}Ta_2O_5$ MFIM system versus the domain wall coupling factor k for a uniform distribution acceptor type traps (extending for 3.2eV below the Ta_2O_5 conduction band minimum) and for an energy spacing ΔE=7.5 meV. The bias independent emission rate is $e_{n0}{=}5.0{\cdot}10^7$ s^{-1}. All other parameters are as in Fig.2(c), except for the Ta_2O_5 thicknesses that is set to t_D=5nm. Area A=2500nm^2 and n_D=100. **b.** Charge versus ferroelectric field of the $Hf_{0.5}Zr_{0.5}O_2{-}Ta_2O_5$ MFIM system for two different oxide thicknesses, t_D, and different trap densities N_T.

S7 Numerical methods

Numerical integration of Landau–Ginzburg–Devonshire dynamic equations. In this work the integration of the LGD equations is obtained with a specifically tailored implicit integrator with an adaptive error control.

The implicit method has been chosen for two main reasons: a) the inherent numerical stability that allows us to use larger time steps compared to an explicit method; b) the robustness and effectiveness for the solution of numerically stiff problems having largely different time constants.[3] The problem at study is in fact numerically stiff for simulations including interface traps, whose time constants vary in a large range depending on the trap energy and applied bias, and can be very different compared to the ferroelectric time constants.[4]

More specifically, we employed a second-order algorithm, namely the trapezoidal numerical integration method (also known as Crank–Nicolson method), that solves a differential equation $\frac{dx}{dt}=f(t,x)$ in time domain by using $x_{n+1}=x_n+\frac{h}{2}[f(t_n,x_n)+f(t_{n+1},x_{n+1})]$,[5] where f is a generic function of time and of a state variable x, and $h=t_{n+1}-t_n$ is the time step. Because the above expression for x_{n+1} involves variables evaluated at the instant t_{n+1} both at the right- and at the left-hand side, at each integration step it is also required to solve a non-linear system of equations with a Newton–Raphson method, which involves itself the computation of the Jacobian matrix.

The error control, based on the number of the iterations of the Newton–Raphson algorithm, efficiently and automatically adapts the time-step h to achieve a given accuracy for the results, thus allowing very fast simulations and overcoming the computational burden introduced by the resolution of the non-linear system.

Three-dimensional electrostatics simulations. For the MFIM capacitor sketched in Fig.1(a) the polarisation in each domain and the external voltage V_T are the electric field sources of a three-dimensional (3D) electrostatic problem. In order to tackle such a 3D problem and eventually calculate the capacitances defined in Eq.S4, we used an on purpose developed simulation tool.

More precisely, we solve the following electrostatic problem in a connected region Ω of the 3-D Euclidean space

$$\begin{cases} \operatorname{curl}\bar{E} &= \bar{0} \\ \operatorname{div}\bar{D} &= \rho \\ \bar{D} &= \varepsilon\,\bar{E}, \end{cases} \tag{S17}$$

where ε is the electric permittivity, $\bar{E}$ and $\bar{D}$ are the electric field and the electric displacement vectors, respectively. The material parameter ε is assumed to be a positive scalar value which is piecewise uniform in each material region. The region boundary $\partial\Omega$ is partitioned into a set of $N^{\mathrm{c}}+1$ disjoint equipotential surfaces *(electrodes)* of perfect metals $\partial\Omega_k^{\mathrm{c}}$ and a set of N^{i} surfaces where the normal component of the electric field vanishes:

$$\partial\Omega=\sum_{k=0}^{N^{\mathrm{c}}}\partial\Omega_k^{\mathrm{c}}+\sum_{k=1}^{N^{\mathrm{i}}}\partial\Omega_k^{\mathrm{i}}. \tag{S18}$$

Electrode $\partial\Omega_0^{\mathrm{c}}$ is considered as reference for all the voltages of the remaining electrodes, that are supposed to be assigned. $\bar{D}\cdot\bar{n}=0$ is set as boundary conditions on each $\partial\Omega_k^{\mathrm{i}}$, where $\bar{n}$ is the outwards oriented normal unit vector of $\partial\Omega$.

The solver implements an electrostatic formulation based on the electric scalar potential,[6] that expresses physical laws directly in an algebraic form by using tools from algebraic topology. Physical variables are defined as fluxes or circulations on oriented geometric elements of a pair of dual interlocked computational grids, while physical conservation laws are enforced strongly in a metric-free fashion by means of incidence matrices between grid elements. The metric and the material information are encoded in the discrete counterpart of the constitutive laws of materials, also referred to as material matrices. The stability and consistency of the method are guaranteed by precise properties (symmetry, positive definiteness, geometric consistency) that material matrices have to fulfill.

The main advantage of this approach with respect to the conventional Finite Element Method is that the material matrices for arbitrary polyhedral elements can be geometrically defined, by simple closed-form expressions, in terms of the geometric elements of the primal and dual grids.

References

[1] M. Hoffmann, M. Pešić, S. Slesazeck, U. Schroeder, and T. Mikolajick, "On the stabilisation of ferroelectric negative capacitance in nanoscale devices," *Nanoscale*, vol. 10, pp. 10 891–10 899, 2018. doi: 10.1039/C8NR02752H.

[2] A I. Khan, K. C. andJ. P. Duarte, Z. Lu, A. Sachid, S. Khandelwal, R. Ramesh, C. Hu and S. Salahuddin, "Negative Capacitance in Short-Channel FinFETs Externally Connected to an Epitaxial Ferroelectric Capacitor," *IEEE Electron Device Letters*, vol. 37, no. 1, pp. 111–114, 2016.

[3] G. Dahlquist and B. Lindberg, "On some implicit one-step methods for stiff differential equations," *Tech. Report*, Department of Information Processing, Royal Institute of Technology, Stockholm, 1973.

[4] T. Rollo and L. Daniel and D. Esseni, "Accurate and Efficient Dynamic Simulations of Ferroelectric Based Electron Devices," *2019 International Conference on Simulation of Semiconductor Processes and Devices (SISPAD)*,pp. 1-4, 2019. doi: 10.1109/SISPAD.2019.8870373.

[5] G. Dahlquist, "A Special Stability Problem for Linear Multistep Methods," *BIT Numerical Mathematics*, vol. 3, pp. 27-43, 1963. doi: 10.1007/BF01963532.

[6] R. Specogna, "Complementary geometric formulations for electrostatics," *International Journal for Numerical Methods in Engineering*, vol. 86, pp. 1041-1068, 2011.